

The Resonant Remains of Broken Chains from Major and Minor Mergers

RIXIN LI (李日新)^{1,*} EUGENE CHIANG (蔣詒曾)^{1,2} NICK CHOKSI,¹ AND FEI DAI (戴飞)³

¹*Department of Astronomy, Theoretical Astrophysics Center, and Center for Integrative Planetary Science, University of California Berkeley, Berkeley, CA 94720-3411, USA*

²*Department of Earth and Planetary Science, University of California Berkeley, Berkeley, CA 94720-4767, USA*

³*Institute for Astronomy, University of Hawai'i, 2680 Woodlawn Drive, Honolulu, HI 96822, USA*

(Received –; Revised –; Accepted –)

ABSTRACT

Observations with the *Transiting Exoplanet Survey Satellite* and *Kepler* have revealed that practically all close-in sub-Neptunes form in mean-motion resonant chains, most of which unravel on timescales of 100 Myr. Using a series of N -body integrations, we study how planetary collisions resulting from the destabilization of resonant chains produce the distribution of orbital periods observed among mature systems, focusing on the resonant fine structures that remain post-instability. In their natal chains, planets near first-order resonances have period ratios just wide of perfect commensurability, driven there by disk migration and eccentricity damping. Sufficiently large resonant libration amplitudes (of unknown origin) are needed to trigger instability. Ensuing collisions between planets (“major mergers”) erode but do not completely eliminate resonant pairs; survivors which avoid mergers show up as narrow “peaks” just wide of commensurability in the histogram of neighboring-planet period ratios. Merger products exhibit a broad range of period ratios, with each resonant peak in the histogram spawning a continuum of ratios wide of the given resonance. These continua may fill in period ratios between relatively closely separated resonances such as the 5:4, 4:3, and 3:2, but may fail to bridge the relatively wide gap between the 3:2 and the 2:1. Thus a “trough” manifests just short of the 2:1 resonance (and only the 2:1 resonance), as observed. Major mergers are not perfect, and generate collisional debris which undergoes “minor mergers” with planets, in many cases further widening resonant pairs. With all this dynamical activity, free eccentricities of resonant pairs, and by extension the phases of their transit timing variations (TTVs), are readily excited. Because non-resonant planets are merger products, they are predicted to have higher masses than resonant planets.

Keywords: Exoplanet dynamics (490); N-body simulations (1083)

1. INTRODUCTION

By detecting planetary systems in young stellar clusters, the *Transiting Exoplanet Survey Satellite* (*TESS*; Ricker et al. 2014) has effectively enabled us to travel back in time, to see that most close-in exoplanets, with orbital periods $\lesssim 100$ days, formed in mean-motion resonance. Figure 1, reproduced from Dai et al. (2024), shows that the fraction of neighboring exoplanet pairs that lie near 1st-order resonance, with period ratios

within a few percent of $(m+1):m$ for positive integer m , is as high as $\sim 70\%$ at ages between 10^7 – 10^8 yr. The fraction of systems containing at least one pair in 1st or 2nd-order $[(m+2):m]$ resonance is still higher, $\sim 86\%$. These fractions decline to ~ 15 – 23% at ages $> 10^9$ yr (see also Lissauer et al. 2011; Fabrycky et al. 2014).

Resonances are a smoking gun for migration; it seems clear that close-in exoplanets, most of which are Neptune-sized or smaller, underwent convergent migration in their parent disks and captured themselves into mean-motion resonance, on timescales $\lesssim 10^7$ yr. The occasional resonant pairs that we observe around Gyr-old stars, and the handful of similarly old and spectacularly long resonant chains (e.g. Kepler-60, Jontof-Hutter et al. 2016;

Corresponding author: Rixin Li
rixin@berkeley.edu

* 51 Pegasi b Fellow

Kepler-80, MacDonald et al. 2016; Weissman et al. 2023; Kepler-223, Mills et al. 2016; TRAPPIST-1, Agol et al. 2021; Teyssandier et al. 2022; TOI-178, Leleu et al. 2021; and TOI-1136, Dai et al. 2023), are understood to be the survivors of dynamical instabilities that broke apart primordially long chains on timescales of 100 Myr (e.g. Izidoro et al. 2017, 2021; Goldberg & Batygin 2022).

Our present study seeks to better understand how resonant chains break to give rise to the properties of mature planetary systems. We do not investigate the physical causes of dynamical instability, but concentrate instead on its consequences. We focus on reproducing two observables: the distribution of orbital period ratios P_2/P_1 of adjacent planets (where P_1 is the orbital period of the inner member of a pair, and P_2 the period of the outer member), and the transit timing variations of near-resonant pairs.¹ The former is displayed in the bottom panel of Figure 2, plotted for planets with radii $< 4R_\oplus$ orbiting Gyr-old stars surveyed by *Kepler*, as drawn from the March 2024 NASA Exoplanet Archive. The salient features of the P_2/P_1 period ratio histogram are: (i) a broad continuum of values atop of which are (ii) excess populations near 1st-order commensurabilities, 3:2 being the most prominent, followed by the 2:1, 4:3, and 5:4, all of which have (iii) a preference for period ratios slightly wide of perfect commensurability. For positive integers p and q , the fractional deviation from a perfect $p:q$ period commensurability is measured by

$$\Delta \equiv \frac{q P_2}{p P_1} - 1. \quad (1)$$

The resonant “peaks” in the histogram have $\Delta \sim +1\%$ (histogram bins in Figure 2 have widths of 2%). The 2:1 peak—and notably not the other peaks at 3:2, 4:3, and 5:4—is accompanied by a “trough” (a population deficit) at $\Delta \sim -1\%$. Peak-trough structures are formed from dissipative processes like stellar tides (Lithwick & Wu 2012; Batygin & Morbidelli 2013) and dynamical friction exerted by parent disks (e.g. Choksi & Chiang 2020)—any process that drives pairs to their resonant fixed points, which naturally lie at $\Delta > 0$ (because resonant orbits apsidally regress; see the introduction of Choksi & Chiang 2020 for details). We will examine whether these structures in the P_2/P_1 histogram can survive, or be created by, the dynamical upheavals that broke resonant chains.

¹ In this paper, unless otherwise indicated, we use the terms “resonant” and “near-resonant”, and “resonance” and “commensurability”, interchangeably. Often we care only that a pair has a period ratio close to (within a few percent of) an $(m+1):m$ or $(m+2):m$ commensurability, and not necessarily whether its resonant argument is librating or circulating.

For the other observable—transit timing variations (TTVs) in mature resonant pairs—we restrict our attention to TTVs that vary sinusoidally, which requires that pairs be sufficiently isolated from other mean-motion resonances with other planets. For sinusoidal TTVs, “phases” can be evaluated (Lithwick et al. 2012; Choksi & Chiang 2023). The TTV phase measures “free” eccentricities, i.e., the components of the eccentricity vector that are specified by initial conditions and not by the mutual forcing between bodies (by analogy to the free and forced components of a driven harmonic oscillator). The larger the free eccentricities, the more the resonant argument varies with time; the pair may be in large-amplitude libration or circulation. Eccentricities and periape longitudes, and by extension resonant arguments, are difficult to measure from transit measurements alone, and thus the TTV phase (the measurement of which we will describe in section 4) serves as a convenient proxy for free eccentricity and libration/circulation. The observational puzzle to explain is why observed TTV phases are large ($\gtrsim 1$ rad in magnitude; Lithwick et al. 2012; Hadden & Lithwick 2014; Choksi & Chiang 2023), when dissipative processes like disk-driven migration and eccentricity damping—which otherwise adequately explain peak-trough structures in the P_2/P_1 histogram (Lithwick & Wu 2012; Batygin & Morbidelli 2013; Choksi & Chiang 2020)—would damp away free eccentricities and by extension TTV phases. The dynamical instabilities that dissolved resonant chains are obvious suspects for exciting TTV phases, and we will bring them in for questioning.

Our main interrogation tool is N -body integrations. These are staged after planets form and assemble into resonant chains, last 100 Myr in disk-free environments (we would integrate for longer if not for the computational cost), and involve hundreds to thousands of variously initialized multi-planet systems to statistically survey the chaotic evolution in phase space. We do not model the earlier phase of planet formation in disks (cf. Izidoro et al. 2017, 2021), nor do we attempt to dissect mechanisms for instability (cf. Goldberg et al. 2022). Instead we experiment with different post-disk initial conditions to try to identify those needed to generate instability and reproduce the observations. Instability and orbit crossing lead, for sub-Neptunes this deep in the star’s potential well, to planetary collisions. We follow the outcomes of mergers, and experiment with a rudimentary treatment of planetesimal debris created from mergers, inspired by Wu et al. (2024) who point out how peak-trough structures and TTV phases may arise from scattering of debris. The evolutionary era we are attempting to simulate is akin to that of the “giant impacts” phase in

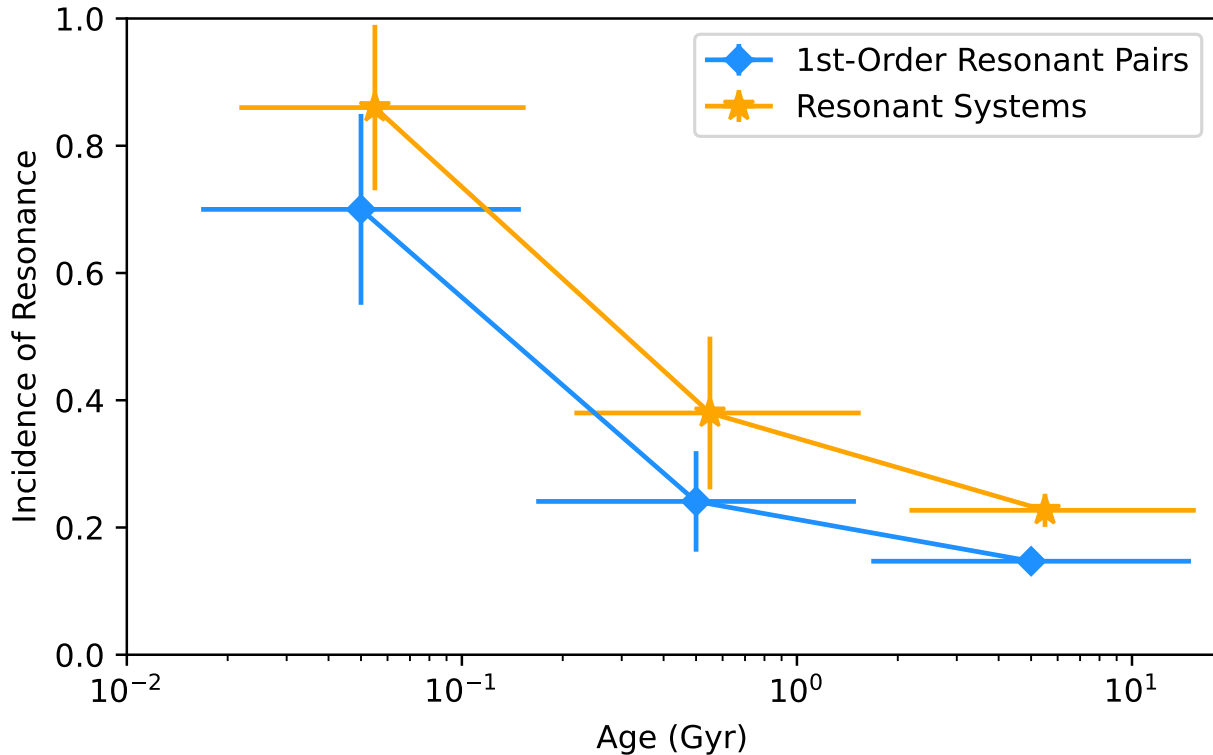


Figure 1. Reprinted from Figure 7 of Dai et al. (2024): the observed decline with age of the fraction of neighboring planet pairs in 1st-order resonance (blue diamonds), and the concomitant decline in the fraction of planetary systems containing at least one pair in a 1st or 2nd-order resonance (orange stars, offset from blue diamonds for clarity). Dai et al. (2024) classify a pair as being in 1st-order resonance if $-0.015 \leq \Delta \leq 0.03$, and in 2nd-order resonance if $-0.015 \leq \Delta \leq 0.015$.

our Solar System (see the review by Gabriel & Cambioni 2023). Our work is in the same vein as Goldberg & Batygin (2022), who ask whether instabilities and the mergers resulting therefrom can explain the claimed intra-system uniformity of *Kepler* planets. These authors also examined the observed distribution of period ratios; our analysis will be more pointed as we focus on the finer structures in the period histogram (in particular the 2:1 peak-trough asymmetry).

As a simplification, we adopt as our template for initial conditions the real-life resonant chain TOI-1136 (Dai et al. 2023). This six-planet chain is attractive for several reasons. It features the most populous resonances observed among (mature) *Kepler* planets, the 3:2 and 2:1, in about the right proportions (three 3:2 vs. one 2:1). It is ~ 700 Myr old, an order of magnitude younger than other resonant chains like TRAPPIST-1 and TOI-178, and its properties are therefore arguably more reflective of formation conditions. Also, unlike other chains, it enjoys the most complete, publicly available set of

vettted orbital elements (including mean anomalies). In this last regard, the orbital eccentricities of TOI-1136 are several times larger than those of other resonant chains, which promotes instability (as we have verified by direct experimentation). We will leverage the work of Dai et al. (2023), who provide a number of disk-planet simulations designed to reproduce TOI-1136 (their section 6.3), plus a convenient set of possible ranges for its orbital parameters (their Table 10). In using TOI-1136 as a basis for our long-term integrations, we are assuming a kind of ergodic hypothesis, that an individual system (or in our case, slightly different variants of an individual system) can, over time, access the same phase space available to a diverse ensemble of systems. Focusing on a single orbital architecture allows for greater experimental control, and simplifies analysis.

This paper is organized as follows. We begin in section 2 with an *a priori* approach, initializing our N -body integrations with the results of disk-migration and eccentricity damping simulations from Dai et al. (2023)

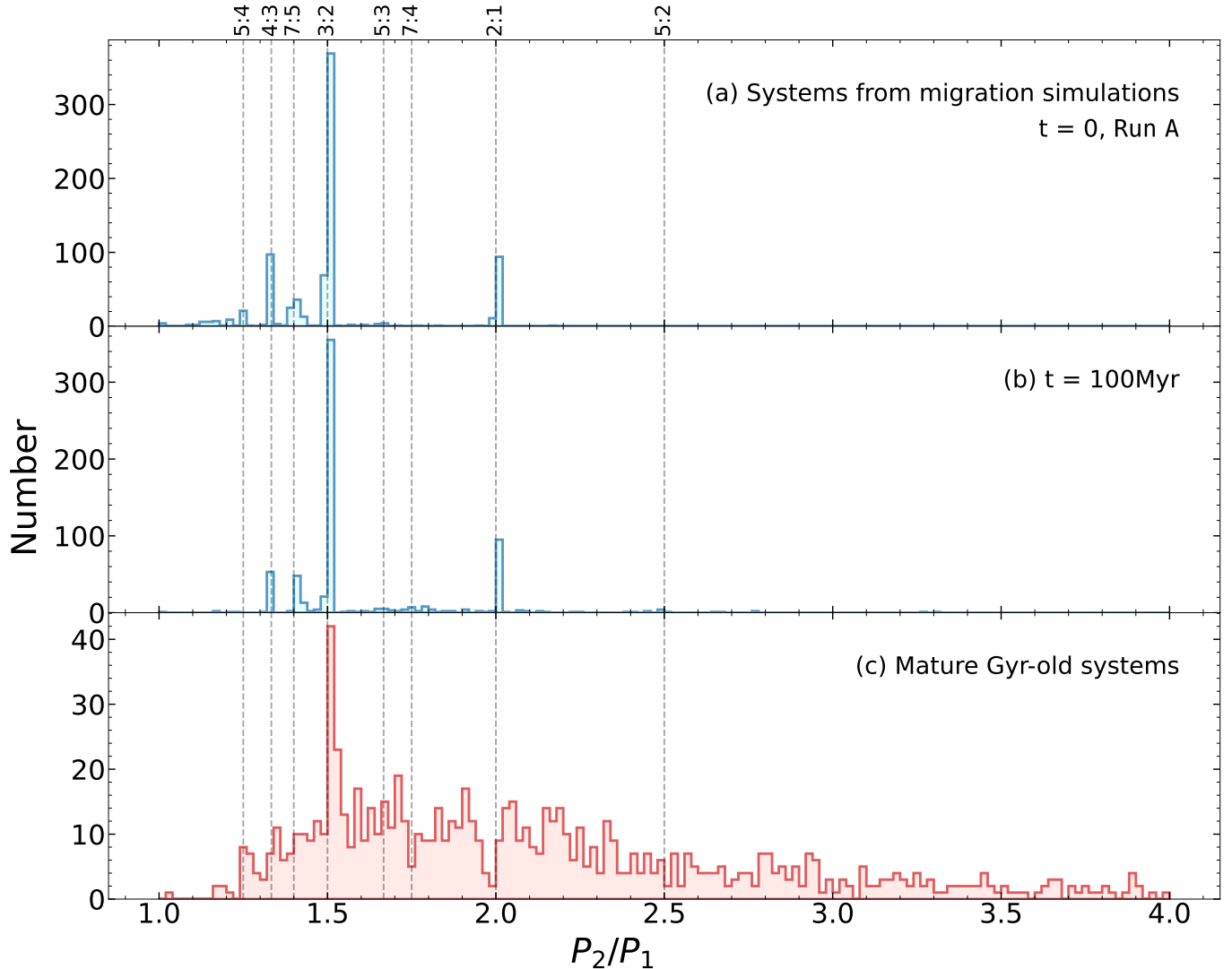


Figure 2. Period ratios P_2/P_1 of neighboring planets, either observed today for planets with radii $< 4R_\oplus$ in the March 2024 NASA Exoplanet Archive (bottom panel), or simulated from Run A, which is initialized with TOI-1136 analogues from the disk-planet simulations of D23 (top panel), and integrated for 100 Myr (middle panel). The Run A systems mostly do not change over time; they are too tightly locked in resonance. The histogram bins have widths of 0.02.

that reproduce TOI-1136 to varying degrees. From these integrations we will see whether we can reproduce the observed decline in resonance occupation (Fig. 1), and the various observed features of the P_2/P_1 period ratio histogram for mature planets (bottom panel of Fig. 2). In section 3, we try a semi-empirical approach, basing our N -body integrations directly on observed orbital elements of TOI-1136, and in particular their ranges as allowed by observational uncertainty. This approach will prove more fruitful, and we will experiment with further variations in initial conditions, and include “minor mergers” with planetesimal debris generated from “major mergers” between planets, to better reproduce the P_2/P_1 histogram. Section 4 compares our predicted TTV phases with those observed. We conclude in section 5.

2. LONG-TERM INTEGRATIONS STARTING FROM MIGRATION SIMULATIONS

Our first experiment is based on the disk migration simulations of Dai et al. (2023, hereafter D23), intended to reproduce the orbital architecture of TOI-1136 (see our introduction). These simulations (which adopt the first migration prescription in section 6.3 of D23; see also their Figure 10) modeled short-scale, Type-I (inward) migration and eccentricity damping of six planets, and yielded an ensemble of $N = 160$ coplanar resonant chains

Table 1. 100-Myr Integrations

Run	Setup	N
A	Analogues of TOI-1136 from migration and eccentricity damping simulations in D23 , first prescription of their section 6.3	160
B	Analogues of TOI-1136 from best-fit observations and uncertainty ranges in D23 , using Δ_+ in Table 2	256
B1	Similar to B but replacing e:f=7:5 with e:f=3:2	256
B2	Similar to B but replacing e:f=7:5 with e:f=2:1	256
B3	Similar to B but with initial eccentricities damped to < 0.01	256
C	Similar to B but with $N_{\text{debris}} = 30$ coplanar debris particles generated per major merger	256
D	Similar to C but with debris particles isotropically ejected in 3D	256

Table 2. Observed ([D23](#)) and Adjusted Period Ratios in TOI-1136

	b:c	c:d	d:e	e:f	f:g
$P_2 : P_1$	1.4995	2.0008	1.5016	1.3999	1.5024
Commensurability	3:2	2:1	3:2	7:5	3:2
Δ	-0.00031	+0.00039	+0.00107	-0.00010	+0.00163
Δ_+ values adjusted by hand to be > 0 and used to initialize Runs B-D					
Δ_+	+0.00100	+0.00039	+0.00107	+0.00010	+0.00163

following the parking of the innermost planet b at the inner disk edge. The top panel of [Figure 2](#) shows the distribution of period ratios P_2/P_1 in the 160 systems constructed across disk parameter space (varying disk mass and scale height and thus migration and eccentricity damping rates). Most pairs are captured near first-order commensurabilities: 2:1, 3:2, 4:3, 5:4, and so on. Note how the peaks near the 2:1 and 3:2 resonances lie preferentially at larger P_2/P_1 (i.e. $\Delta > 0$), as expected from eccentricity damping (e.g., [Choksi & Chiang 2020](#)). A second-order 7:5 resonance is exhibited in 75 out of 160 chains, with 63 having the same sequence of resonances as in TOI-1136 (3:2, 2:1, 3:2, 7:5, 3:2). Second-order resonances are generated by relatively slow migration in low-mass disks.

We use the results of these 160 disk-migration simulations as initial conditions for our post-disk integrations (**Run A** in [Table 1](#)). We integrate each six-planet system, disk-free, for 100 Myr using the REBOUND code ([Rein & Liu 2012](#)) outfitted with the hybrid-symplectic MERCURIUS integrator ([Rein et al. 2019](#)) (similar results were obtained with the TRACE integrator; [Lu et al. 2024](#)). For planets like those in TOI-

1136 whose orbital velocities exceed their surface escape velocities, dynamical instability and orbit crossing should lead to collisions and mergers, rather than ejections from the host star (e.g., [Goldreich & Sari 2003](#)). Unlike the original [D23](#) simulations, we allow for planetary collisions by assigning non-zero physical radii R_p to the planets (see [Table 10](#) of [D23](#)). In **Run A** (and also in the later **Run B** series), planetary collisions are assumed to result in perfect mergers conserving mass and momentum, with merger products assigned a new physical radius $R_{\text{merger}} = (R_1^2 + R_2^3)^{1/3}$. Over the last 4.1 years of the integrations (the *Kepler* mission duration), we measure the orbital periods of allplanets using mock transit observations.

As displayed in [Figure 2](#), the final distribution of neighboring-planet period ratios P_2/P_1 at $t = 100$ Myr is mostly unaltered from its initial distribution at $t = 0$. In particular the final period ratio distribution lacks the continuum of values observed for mature *Kepler* systems (at $t \sim$ several Gyrs). Mostly what happens over 100 Myr is the destruction of the closest resonant pairs (5:4 and narrower, and about half of the 4:3 population), which are unstable without eccentricity damping from

the parent disk. The planets initially captured into 3:2, 2:1, and 7:5 resonance largely stay there.

Our inability to reproduce the observed secular decline in resonance occupation (Fig. 1) using the migration simulations of D23 implies that these simulations, which are typical of those in the literature, do not statistically represent the orbital configurations of young systems after disk dispersal. For the remainder of this paper we try a different approach.

3. A SEMI-EMPIRICAL APPROACH: LONG-TERM INTEGRATIONS STARTING FROM OBSERVATIONS

The null results from the previous section imply that there must be physical effects missing from standard disk-migration and eccentricity damping simulations in assembling and shaping resonant chains. There does not seem to be consensus as to what these are; candidates include stochastic torques from disk turbulence (e.g. Rein & Liu 2012; Goldberg & Batygin 2023), mass loss from planetary gas envelopes (Matsumoto & Ogihara 2020; Owen & Schlichting 2024), overstable librations from eccentricity damping (Goldreich & Schlichting 2014; Nesvorný et al. 2022), or scattering and collisions from planetesimals (Wu et al. 2024). Rather than investigate this issue from first principles, we take a different tack, leveraging the observations in an admittedly ad hoc and arbitrary manner to explore possible post-disk initial conditions. We rely again on TOI-1136 as a guide, but now construct an ensemble of six-planet systems by uniformly drawing orbital elements within the one-sigma uncertainties of TOI-1136’s observed best-fit parameters (D23, Table 10). These elements cover substantially more parameter space than the simulation-based elements in Run A, and are assumed to embody whatever (unknown) perturbations stirred up resonant chains to the point of breaking. The goal is not to decide what physical effects are responsible for breaking chains, but to study how they break if they break, and how observations may be reproduced. The philosophy is similar to that of Goldberg & Batygin (2022); we will recover similarly positive results, and fill in more details regarding resonant sub-structures in the distribution of period ratios.

We modify this observation-based set of initial conditions in one respect: where $\Delta < 0$, we change the orbital period ratio to $\Delta > 0$. We do this for two reasons. First, disk migration with eccentricity damping predicts planets resonantly capture to $\Delta > 0$, for first-order resonances in a time or ensemble-averaged sense (e.g., Choksi & Chiang 2020, and our Figure 2). Second, we found upon experimentation that when our initial conditions follow the preference for $\Delta < 0$ as per the D23

observations of TOI-1136, the final Δ distribution after integration preserves the preference for $\Delta < 0$, contrary to observation.

Thus, for the innermost 3:2 b:c pair, we do not use the observed best-fit $\Delta = -0.00031$, but instead use $\Delta_+ = +0.001$ (similar to the observed $\Delta = +0.00107$ for the other 3:2 d:e pair in the system; see Table 2). We make a similar replacement for the 7:5 e:f pair, flipping the sign of the initial Δ from -0.0001 to $+0.0001$ (though capture into second-order resonance has not been shown to favor $\Delta > 0$). To calculate the initial orbital periods (semi-major axes) for the six planets, we first set the orbital period of planet b to its observed best-fit value of 4.17278 days (D23 Table 10), and then use the Δ_+ values in our Table 2 to determine the remaining orbital periods. All other orbital parameters (planet-to-star mass ratio, mean anomaly, eccentricity, longitude of pericenter) are sampled independently and within the ranges listed in Table 10 of D23. Our independent sampling ignores correlations between fitted elements, and thus surveys a large volume of parameter space in which there is no guarantee of stability.

Altogether we construct $N = 256$ coplanar TOI-1136 clones for 100-Myr integrations with MERCURIUS, assuming perfect mergers — this experiment constitutes our Run B.

The top two panels of Figure 3 show the initial and final P_2/P_1 distributions. In contrast to Run A, many of the resonant chains in Run B break. They break when a pair of planets stir each other to sufficiently large eccentricity that they collide and merge. The merger product tends to have an orbital period intermediate between that of the colliders, widening adjacent orbital spacings. Thus, if planet e collides with f, in addition to the e:f = 7:5 resonance being destroyed, the resultant period ratio between d and the merger product ef increases from the original d:e=3:2, and similarly the period ratio between the merger product ef and g increases from the original f:g = 3:2. In this way pairs initially in the 3:2 resonant peak are displaced to a broader continuum of values $P_2/P_1 > 3/2$ in Figure 3 — see the light orange blocks marked ‘ef’ in Figure 4, which pair with either the dark purple blocks marked ‘d’ or the grey blocks marked ‘g’. Similarly, a second continuum of $P_2/P_1 > 2$ ratios is created from mergers of b and c.

Intriguingly, and perhaps by chance, the first continuum falls just short of $P_2/P_1 = 2$, creating a “peak-trough” structure near the 2:1 resonance like the one observed for mature systems. The initial 7:5 pairs appear largely eliminated, also in agreement with *Kepler* statistics. One problem is that some of the b:c = 3:2 pairs that survive appear to have evolved to $\Delta < 0$,

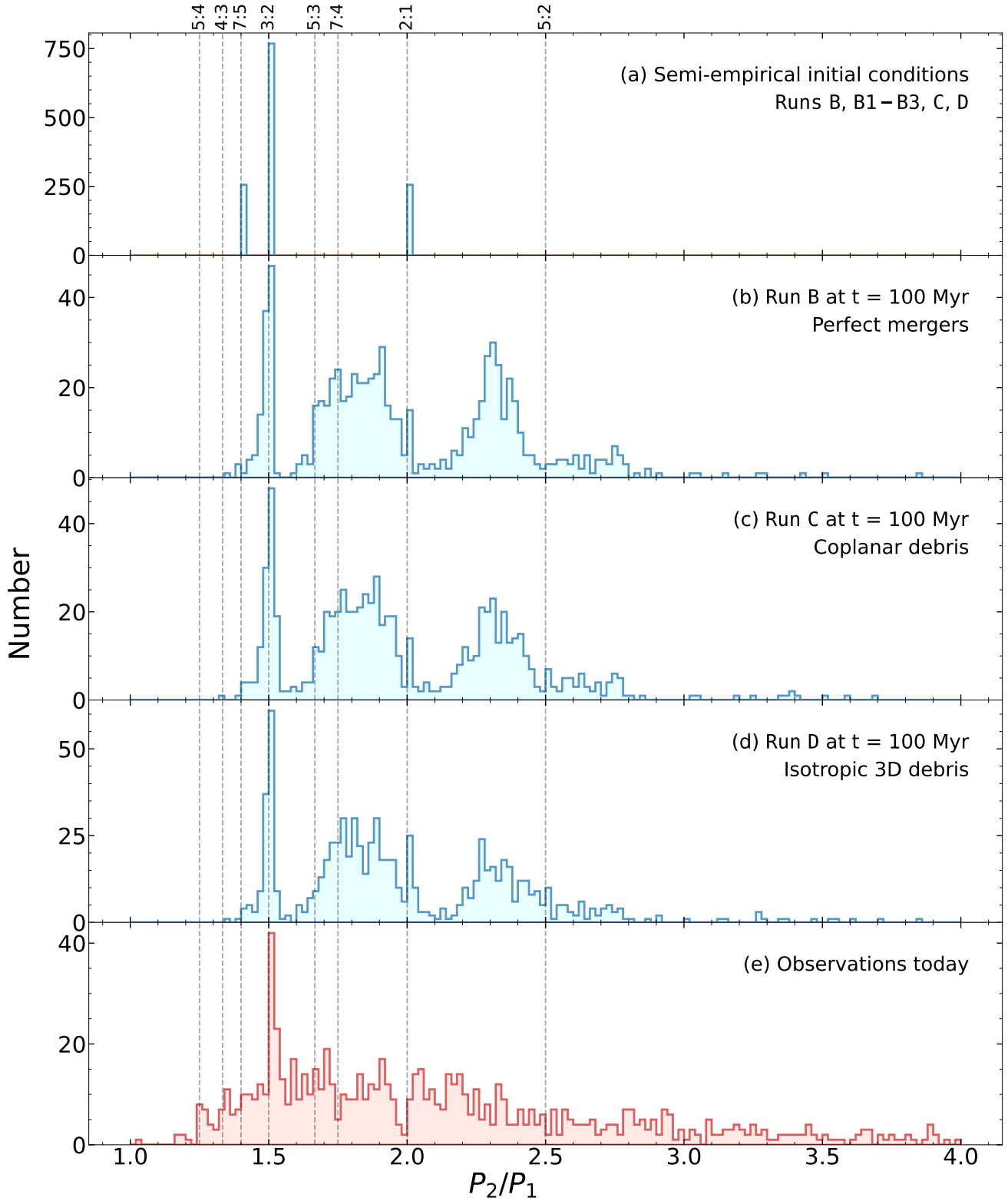


Figure 3. Neighboring planet period ratios for (a) our semi-empirical Runs B–D at the start of our integrations (note how all pairs are initialized with $\Delta_+ > 0$; see Table 2); (b) the final state of Run B, which assumes collisions result in perfect mergers; (c) the final state of Run C, where major mergers produce coplanar debris particles that undergo scattering and minor mergers; (d) the final state of Run D, where major mergers produce debris particles ejected isotropically in 3D; and (e) the observations as downloaded for planets with radii $< 4R_\oplus$ from the NASA Exoplanet Archive in March 2024.

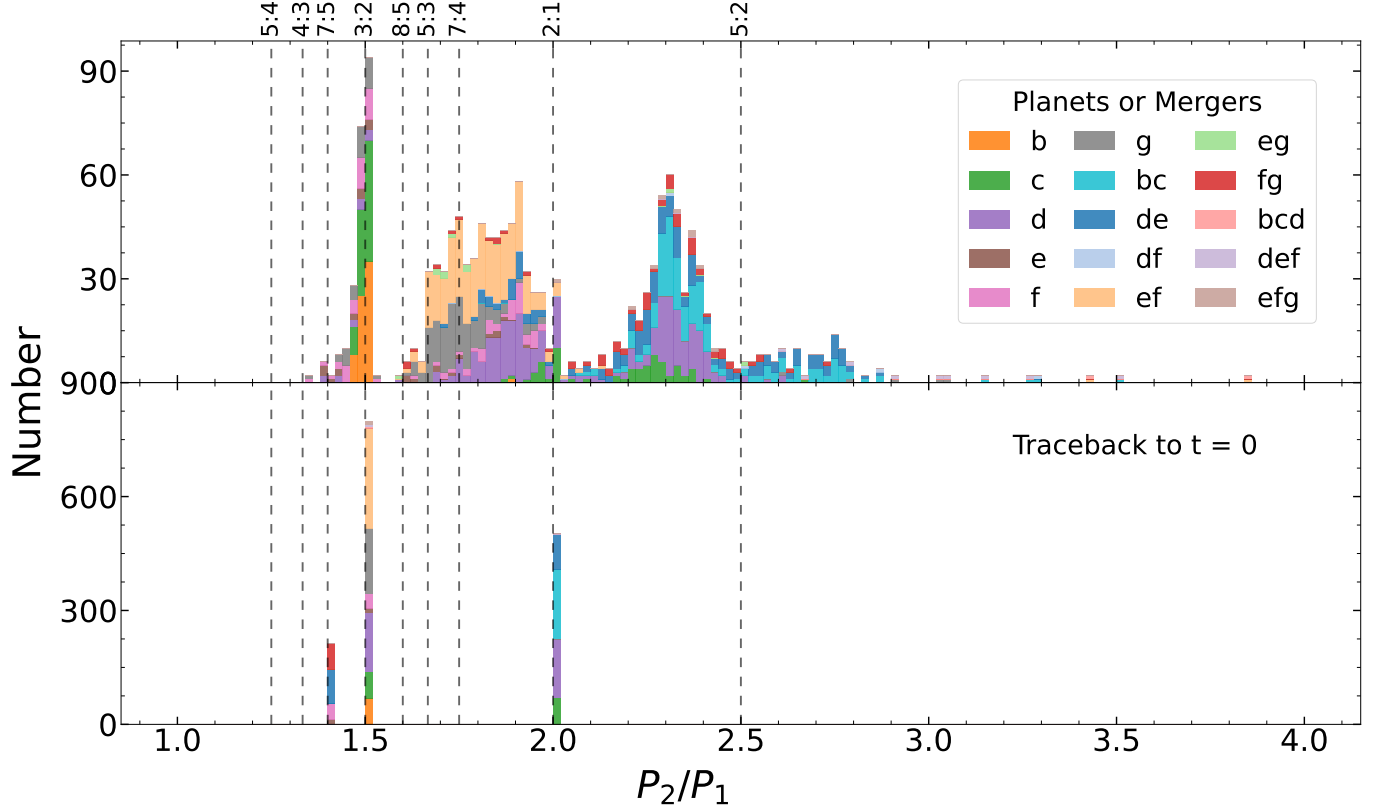


Figure 4. A history of violence: how planetary mergers alter period ratios. Top panel: the final P_2/P_1 distribution at $t = 100$ Myr for **Run B**, color-coded according to the planets that contribute to a given period ratio. Combined letters denote a merger product; e.g., ‘bc’ indicates the merged product of planets b and c, and ‘bcd’ the merger of planets b, c, and d. Since every period ratio involves two planets, the histogram in the top panel is twice the height of the histogram for **Run B** as shown in the second panel of Figure 3. Bottom panel: tracing the planet pairs contributing to a given period ratio at $t = 100$ Myr back to their original period ratios at $t = 0$. If a pair at $t = 100$ Myr involves merger products, we assign both members of the pair to the original period ratio that connects the pair; thus, e.g., a pair consisting of planet d and merger ef in the top panel are mapped to the original period ratio between d and e ($3/2 + \Delta_+$) in the bottom panel, and not the ratio between e and f ($7/5 + \Delta_+$). In this way, we have a one-to-one correspondence between the two panels, excepting the rare mergers of non-neighboring planets (4 df and 10 eg planets) for which assigning unique initial period ratios is too ambiguous.

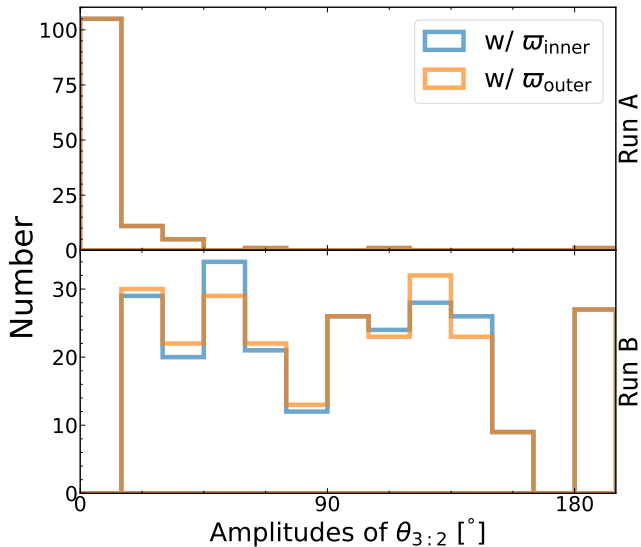


Figure 5. Initial 3:2 resonant libration amplitudes of the innermost b:c planet pairs for Run A (top panel) and Run B (bottom panel). There are two resonant arguments for the co-planar 3:2 resonance, one which depends on the longitude of periapse of the inner planet b (blue histogram), and another which depends on that for the outer planet c (orange histogram). Libration amplitudes are determined by sinusoidal fits to the resonant argument vs. time, and evaluated as the deviation from libration center. In the top panel, only the 124 systems (out of a total of 160 in Run A) that have the b:c pair near a 3:2 resonance are plotted, and of these only 1 system is in circulation, which we assign a libration amplitude of 180° . For the observation-based simulations in Run B, 27 out of 256 systems are in circulation, including those that switch between libration and circulation. The larger initial libration amplitudes in Run B explain why its resonant chains break more easily than those in Run A.

in a proportion that seems too large to compared to observations of mature systems.

Dynamical instabilities in Run B, and their absence in Run A, can be attributed to differences in their initial resonant libration amplitudes, as shown in Figure 5 for the innermost b:c = 3:2 pairs. Larger libration amplitudes in Run B stem from the observational uncertainties on which this run is based (see also Jensen & Millholland 2022), and permit closer and more varied encounters between planets. For a deeper analysis of the mechanics of instability in chains, see Goldberg et al. (2022).

3.1. Further Experiments Assuming Perfect Mergers (Runs B1-B3)

Runs B1-B3 are variations on Run B. In Run B1 we replace the original e:f = 7:5 resonance with the 3:2 resonance, changing only the period ratio for e:f (and not changing Δ_+ , which remains at 0.0001). All other

parameters (eccentricity, mean anomaly, etc.) are sampled the same way as in Run B. Run B2 is a similar experiment that replaces the e:f 7:5 resonance with the 2:1 resonance. As shown in Figure 6 (second and third panels from the top), the replacement of the 2nd order resonance with a 1st order resonance appears to stabilize the system: apart from some systems spreading to $\Delta < 0$, there are hardly any mergers. It may be that 2nd order resonances, which are intrinsically weaker than 1st order resonances, play a prominent role in breaking resonant chains over time (see also section 7.2 of D23, and Xu & Lai 2017).

In Run B3, before we integrate for 100 Myr, we damp eccentricities using the `modify_orbits_forces` routine in REBOUNDx (Tamayo et al. 2020) and integrate for $10\tau_e = 10e/\dot{e}$, so that all planets have new initial eccentricities < 0.01 (by comparison, in Run B, initial eccentricities range from ~ 0.01 to ~ 0.12 ; D23 Table 10). The resultant systems are completely stable over 100 Myr (Figure 6 bottom panel). Sufficiently large eccentricities—technically free eccentricities that give rise to non-zero resonant libration amplitudes—appear essential for breaking resonant chains.

3.2. Imperfect, Debris-Generating Mergers (Runs C-D)

Mergers are messy, as recently emphasized by Wu et al. (2024, and references therein). Collisions at relative velocities greater than the planets’ surface escape velocities are mostly oblique and hit-and-run (e.g., Aarseth et al. 1993; Leinhardt & Stewart 2012; Cambioni et al. 2019; Emsenhuber & Asphaug 2019; Emsenhuber et al. 2020), producing debris not immediately re-accreted by the colliders. Esteves et al. (2022) simulated imperfect mergers in breaking chains, finding the gross evolution to be largely the same as when mergers are assumed perfect. We will not disagree, but will focus on the effects that debris and imperfect mergers have on the finer resonant sub-structures in the period ratio distribution. Wu et al. (2024) have shown that scattering of planetesimals strewn between and around a pair of resonant planets can wedge them farther apart, potentially explaining the preference for $\Delta > 0$ observed among mature sub-Neptunes.

Accordingly in Runs C and D, we relax the assumption of perfect mergers. Each time two planets collide, the merger product is assumed to contain 90% of the combined mass, with the remaining 10% distributed equally among $N_{\text{debris}} = 30$ new particles. Debris particles carry mass but do not interact with each other; they only interact with planets via gravity, and can collide with planets in subsequent “minor mergers” that are assumed perfect. The debris particles are born with

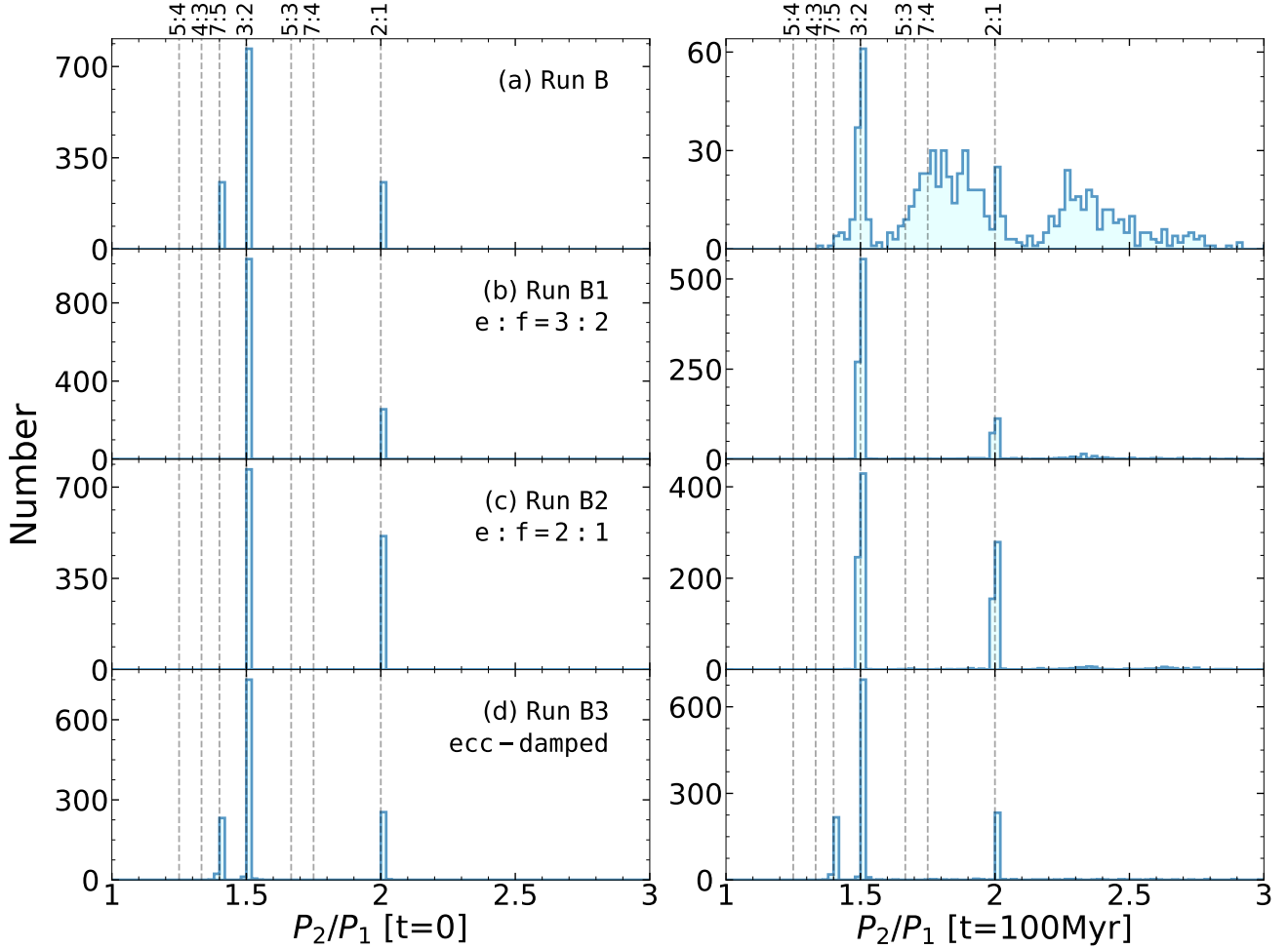


Figure 6. Initial (left column) and final (right column) period ratio distributions for Runs B, B1, B2, and B3 (top to bottom rows; see also Table 1). These experiments demonstrate that the presence of a weak 2nd-order resonance like the 7:5 (absent in Runs B1-B2), and sufficiently large initial eccentricities (absent in Run B3), help promote instability and the breaking of resonant chains.

isotropic ejection velocities. Their initial locations are randomly displaced by $\delta\mathbf{r}$ from the collision site, where $|\delta\mathbf{r}|$ is $50\times$ the physical radius of the merger product, and their initial velocities are those of the merger product plus a velocity $\delta\mathbf{v}$ parallel to $\delta\mathbf{r}$, with $|\delta v|$ equal to 30% of the relative impact velocity between merger progenitors. The above prescription is made more for computational ease than anything else, though the fraction of mass ejected (10%) and the ratio of ejection to collision velocities (30%) do not seem unrealistic for the mass that escapes the gravity well of the merger product (e.g. Esteves et al. 2022; see also Figure 3 of Gabriel & Cambioni 2023, and references therein). To ensure the collision does not alter the planetary system’s center of mass, debris particles are created in diametrically opposed pairs (with $\pm\delta\mathbf{r}$). In Run C, debris particles are restricted to be coplanar with the planetary system ($\delta\mathbf{r}$ traces a circle). In Run D, we allow for 3D motions ($\delta\mathbf{r}$ traces a sphere). For each of

Runs C and D, initial conditions for $N = 256$ TOI-1136 clones are identical to those in Run B (i.e. the same seed random numbers were used to sample initial conditions for all Runs B-D).

Figure 3 compares the post-integration P_2/P_1 ratios for Runs B-D. The results are similar, with Run D arguably yielding a peak-trough 2:1 asymmetry most closely resembling that observed today. The continuum of values at $3/2 < P_2/P_1 < 4$ also slopes more gently downward with increasing period ratio, in a manner similar to the observations, modulo the bimodality of the simulations (see discussion of Run B preceding section 3.1). The simulated 3:2 peaks all seem to have somewhat too many systems at $\Delta < 0$ compared to observations, though this problem appears minimized for Run D. Following the definition of first-order resonance adopted in Dai et al. (2024, i.e., $-0.015 < \Delta < +0.03$), the fraction of first-order resonant pairs is 15.5% for Run B, 16.5% for

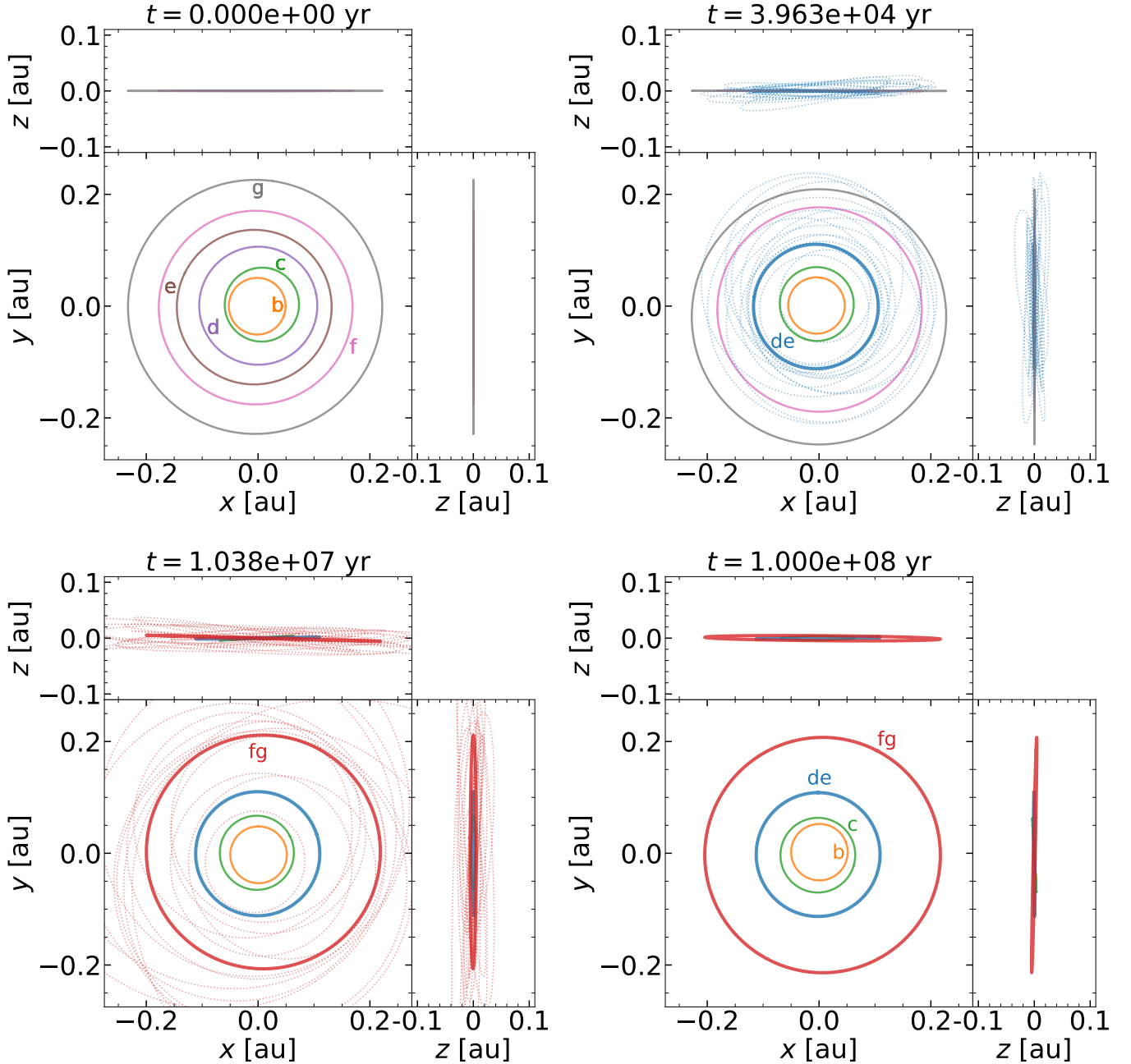


Figure 7. Snapshots seen in various x - y - z projections of one example simulation from Run D, featuring two major merger events at 3.888×10^4 yr (creating planet de) and 1.038×10^7 yr (creating planet fg). The orbits of the initial planets (b, c, d, e, f, and g) are shown in thin solid lines, the orbits of merger products (de, fg) are drawn in thick solid lines, and the orbits of debris particles are plotted in dotted lines with colors that match those of their parent merger products.

C, and 20.8% for D at $t = 100$ Myr. These fractions are comparable to the observed fraction of $\sim 25\%$ for ages 100 Myr – 1 Gyr, as shown in Figure 1. About 1% of the simulated systems survive unscathed to reproduce the same sequence of resonances as in TOI-1136.

Figure 7 shows four snapshots of one of the simulations in Run D. Once created, the debris particles scatter about. Most eventually merge with the parent merger product,

but a fraction are cast more widely. In the example shown, of the 30 debris particles created when planets d and e merge, 21 are accreted by de, 1 collides with b, 2 with c, 4 with f, and 2 with g. Of the 30 debris particles created when f and g merge, 25 are accreted by fg, 3 collide with de, and 2 with c. These minor mergers tend to widen orbital spacings between resonant pairs, insofar as the debris particles just graze the outside

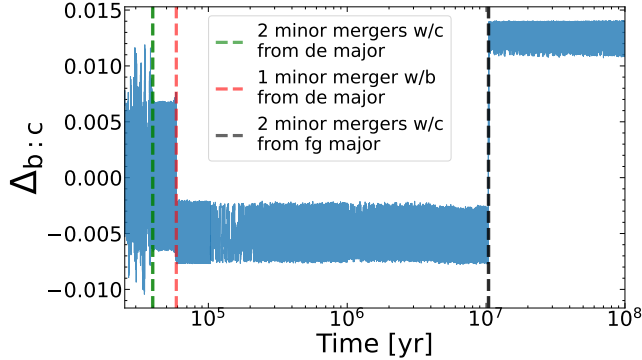


Figure 8. The evolution of Δ for the innermost $b:c = 3:2$ planet pair in the Run D simulation shown in Figure 7. Minor mergers alter Δ , lowering it when a debris particle collides with b (green dashed line), and later raising it when another debris particle collides with c (black dashed line). For the final transit timing variations (TTVs) of this pair, see Figure 11.

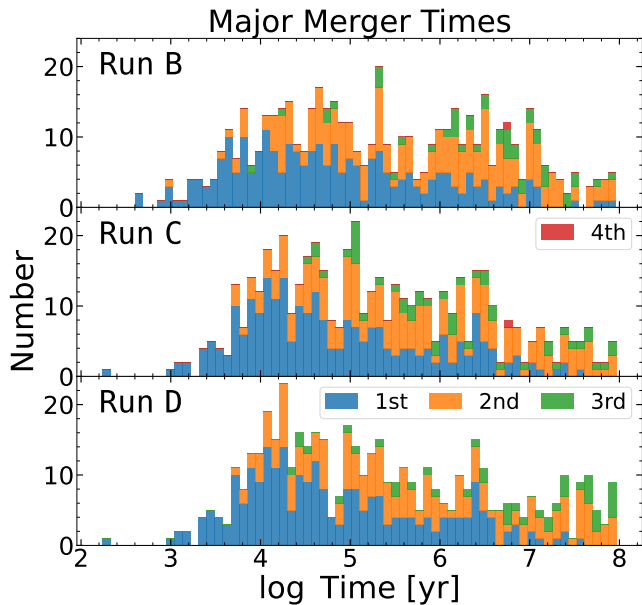


Figure 9. Times when major mergers occur in Runs B–D, color-coded according to whether a merger occurred chronologically 1st, 2nd, 3rd, or (in rare cases) 4th within a given system. Too many resonance-breaking mergers occur at times $< 10^6$ yr to be consistent with the observed decline in resonance fraction over 10^8 yr timescales (Figure 1).

member of the pair (which they do not always do). For example, a debris particle created from the merger of f and g has its eccentricity increased by scattering until its orbit just intersects the orbit of planet c ; the subsequent merger with c widens c ’s orbit (by of order 1%, the mass ratio between the debris particle and the planet) and by extension increases Δ for the $b:c = 3:2$ resonance—see Figure 8 which shows this very evolution, but which also

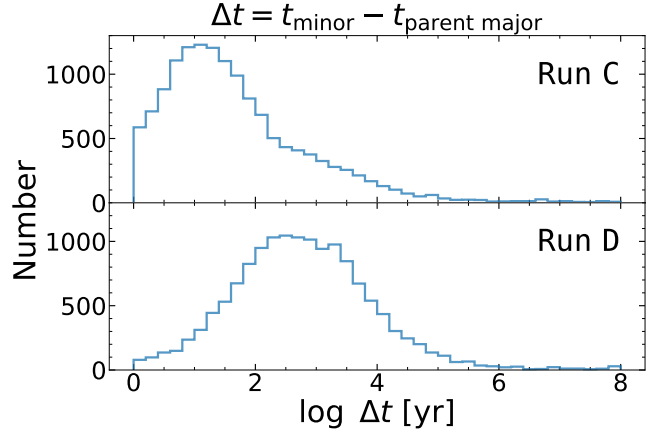


Figure 10. Minor mergers between debris particles and planets occur mostly $\Delta t < 10^4$ yr after the debris particles are born in parent major merger events. Debris particles in Run D are not coplanar with planets and take longer to accrete than in Run C where they are coplanar.

shows that minor mergers do not always unfold this way. Such widening of resonant pairs from “outside grazers” differs from, but complements the widening mechanism of Wu et al. (2024) from planetesimal scattering.

The timestamps in Figure 7 point to a problem with our simulations, which is that the resonances tend to break too soon compared to the $\sim 10^8$ yr timescale over which actual systems are observed to break (Fig. 1). This is a generic problem with Runs B, C, and D. Figure 9 shows that more than half of the major mergers for these runs, out to the fourth merger in a given system, occur at times $< 10^7$ yr. Most systems experience just two mergers, with half of these occurring at $< 10^6$ yr. At $t = 10^6$ yr, the fraction of systems exhibiting at least one 1st or 2nd-order resonance is 47.6%, and the fraction of pairs in 1st-order resonance is 39.6%. These fractions are too low compared to those shown at the earliest times in Fig. 1—this despite our initial conditions being drawn from D23 which ostensibly screened out orbits that were unstable on timescales < 1 Myr (their section 6.1). Probably the appearance here of such short-lived orbits stems from our ignoring correlations when sampling the orbital elements from Table 10 of D23. Minor mergers add negligibly to major merger times—see our Figure 10. To summarize, the dynamical instabilities in our simulations unfold too rapidly to be entirely consistent with Figure 1, which shows $\sim 70\%$ of observed pairs are still in 1st-order resonance at ages as old as 10^7 – 10^8 yr.

4. TTV PHASES

Transit timing variations (TTVs) provide another diagnostic of resonance. A resonant/near-resonant pair of planets sufficiently isolated from other resonances from

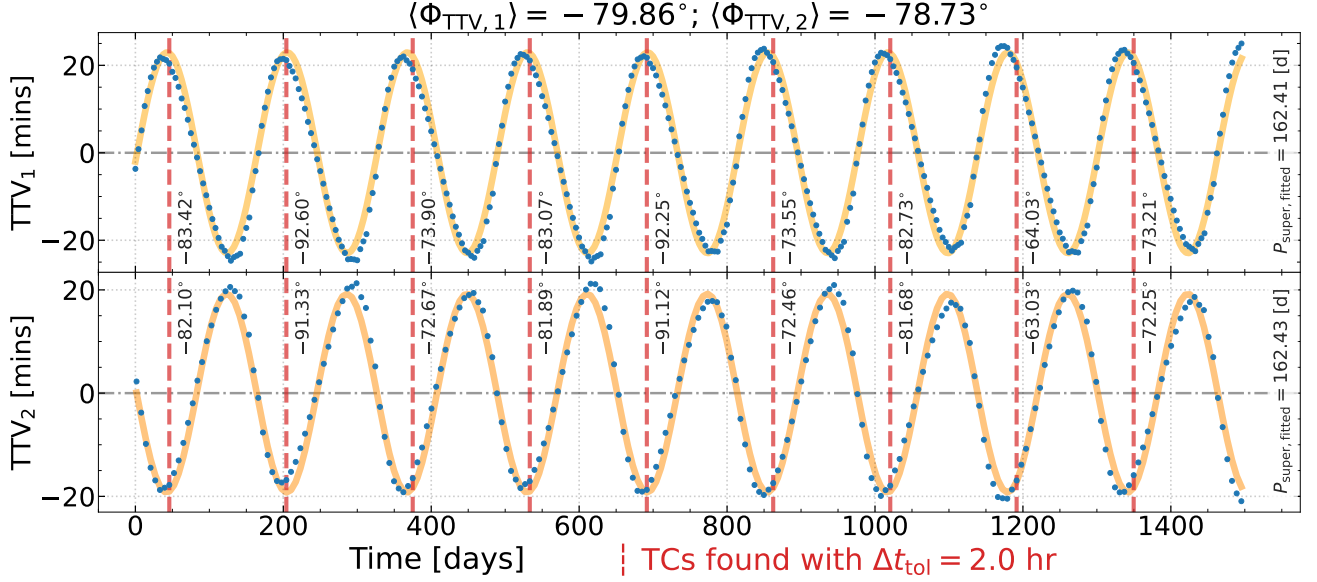


Figure 11. Sample TTV time series from a $b:c = 3:2$ pair at the end of Run D. This pair (subscript 1 for the inner member and 2 for the outer member) has a “well-defined” TTV phase: transiting conjunctions (marked by vertical dashed red lines) occur consistently before TTV zero-crossings with a time-averaged phase difference of $\langle \Phi_{\text{TTV}} \rangle \simeq -79^\circ$. Blue points are simulation data and yellow solid curves are sine-wave fits, with the fitted P_{super} labelled on the right.

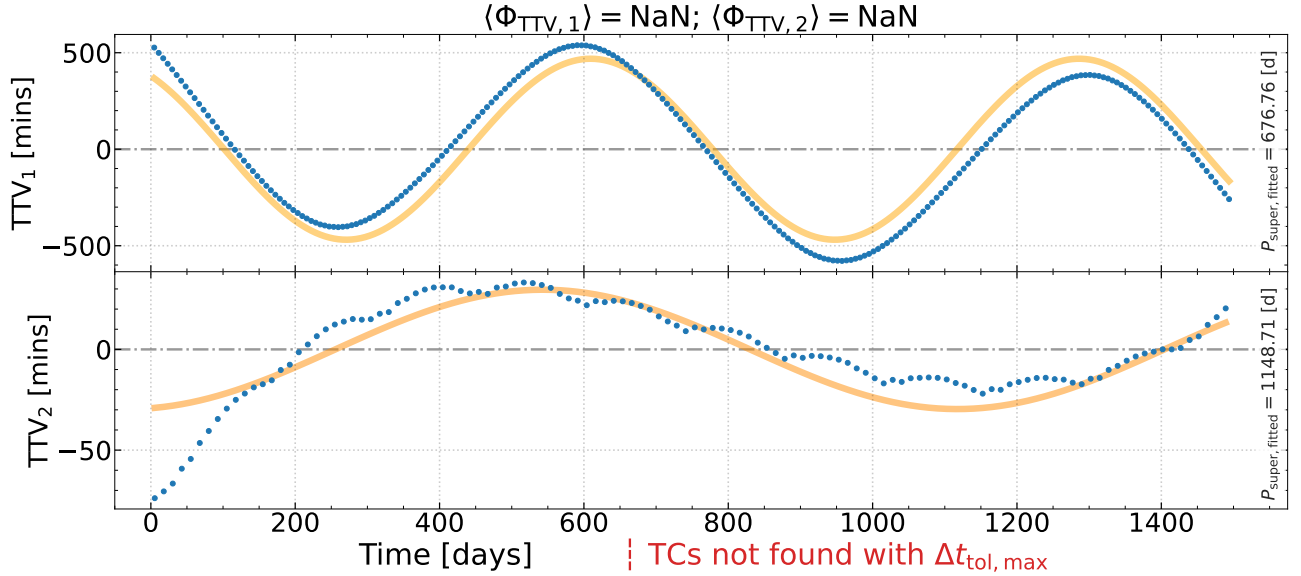


Figure 12. Sample TTV time series for a $c:d = 2:1$ pair for which a TTV phase is not well-defined. The sine-wave fits (yellow solid curves) are poor and yield discrepant values for P_{super} . Also, no transiting conjunction is identified, even using the maximum value of Δt_{tol} .

other planets exhibits sinusoidal TTVs for which a phase, Φ_{TTV} , may be evaluated (Lithwick et al. 2012). The TTV phase is the phase difference between when the two planets transit the star simultaneously (a transiting conjunction, abbreviated as TC) and when the sinusoidal TTV crosses zero (from positive to negative values for the inner planet, and vice versa for the outer; see, e.g., Choksi & Chiang 2023, their figures 2–4). A pair of

planets deeply locked in resonance, with zero libration amplitude—i.e. having purely forced eccentricities, with no free components—has $\Phi_{\text{TTV}} = 0$. Conversely, a circulating or librating pair is free to have $\Phi_{\text{TTV}} \neq 0$.

Observed today, the TTV phases of near-commensurate pairs are distributed broadly from -180° to $+180^\circ$ (Lithwick et al. 2012; Wu & Lithwick 2013; Hadden & Lithwick 2014; Choksi & Chiang 2023),

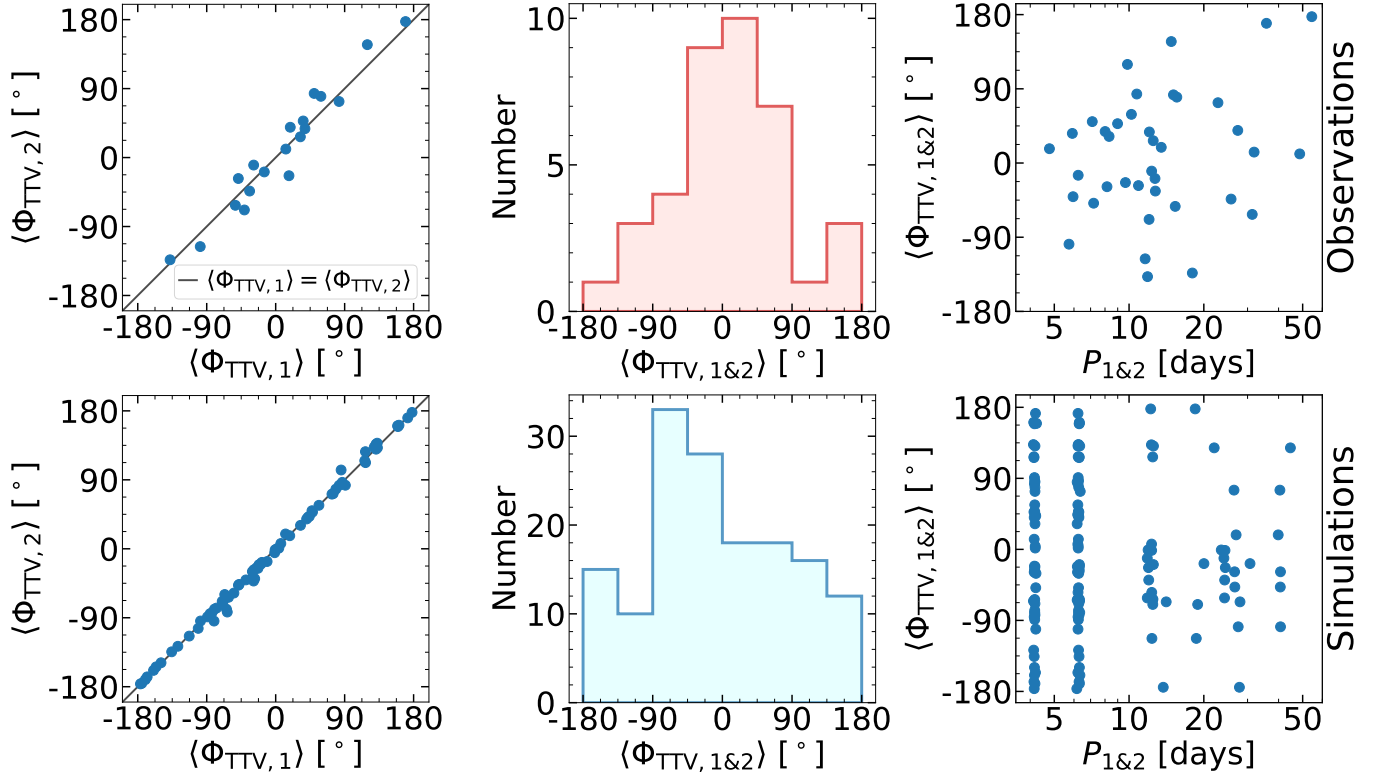


Figure 13. Comparison of time-averaged TTV phases $\langle \Phi_{\text{TTV}} \rangle$ between observations (top row) and Run D simulations (bottom row), for planets with $-0.015 \leq \Delta \leq +0.03$ near the 2:1 and 3:2 commensurabilities (the same Δ criterion for 1st order resonance is used in Dai et al. 2024). Subscript 1 denotes the inner member of the pair, and subscript 2 denotes the outer member. The TTV phases plotted here are all well-defined, i.e. consistent between inner and outer members of pairs (left column). The histograms in the middle column (which plot both $\langle \Phi_{\text{TTV}} \rangle_1$ and $\langle \Phi_{\text{TTV}} \rangle_2$) show encouraging agreement between observed and simulated TTV phases—a concentration near 0° , and broad wings that extend to $\pm 180^\circ$. We detect no trend between TTV phase and orbital period, either in the observations or in the simulations (right column). The simulated resonant pairs all derive from TOI-1136 analogues; most of those with well-defined TTV phases are the innermost surviving b:c = 3:2 pairs. The list of objects/simulations and their TTV phase curves are available [here](#) for the top row and [here](#) for the bottom row.

indicating that many pairs have substantial non-zero free eccentricities. This result is not predicted by dissipative, eccentricity-damping processes, including disk-planet interactions and stellar tides, which can otherwise correctly predict the observed peak-trough asymmetries in the P_2/P_1 histogram (e.g. Lithwick & Wu 2012; Choksi & Chiang 2023). Here we examine to what extent our simulations can resolve this tension.

We calculate Φ_{TTV} for planet pairs near the 3:2 and 2:1 resonances at the end of Run D as follows. For each pair, we perform mock transit observations, fitting the average mean-motion over the last 4.1 years of the integration (the duration of the *Kepler* transit mission) and subtracting off the mean times of transit to obtain each planet’s TTV (the deviation of actual mid-transit time from the mean transit time, vs. time). Each TTV signal is fitted to a sine wave, with amplitude and period determined as part of the fit. The TTV period, sometimes termed the “super-period,” is common to both members of an isolated pair of resonant planets. In our

simulations, sometimes a TTV signal from one member of a pair exhibits two sinusoidal frequencies (due to forcing by other planets), in which case we focus on the frequency component that matches that of the other member of the pair. Times of TCs are then identified as those times when two planets transit the star within some small time interval Δt_{tol} of one another. We start with a maximum value of Δt_{tol} given by the sum of the transit durations, $\Delta t_{\text{tol}} = 2R_\odot(1/v_{K,1} + 1/v_{K,2})$, where R_\odot is the stellar radius and $v_{K,i}$ is the Kepler orbital velocity of planet i . Since this choice sometimes yields multiple TCs per super-period when only one TC is possible, we decrease Δt_{tol} until we can identify as close to one TC per super-period (within the 4.1-yr analysis duration) as possible. Pairs which just have a few missing or extra TCs out of an otherwise good set are kept for analysis. The phase difference between a TC and when the TTV crosses zero (going down for the inner planet, and going up for the outer) is recorded as Φ_{TTV} .

We say that a pair’s TTV phase is “well-defined” if: (a) the sine-wave fit to each member’s TTV time series appears good-by-eye; (b) the best-fit P_{super} from one member matches that of the other member to within 20%; and (c) the mean dispersion in Φ_{TTV} for both members of the pair does not exceed 45 degrees over the 4.1-yr analysis duration (the individual time-averaged $\langle \Phi_{\text{TTV}} \rangle$ of one member of the pair may differ from that of the other). Figure 11 shows the TTV signals from a b:c pair from Run D where Φ_{TTV} is well-defined. By comparison, Figure 12 shows an example where the TTV phase is not well-defined—the sine-wave fit to one of the TTV time series is poor, P_{super} determined from one member of the pair differs from P_{super} determined from the other member by almost a factor of 2, and no TC could be found, not even for $\max \Delta t_{\text{col}}$. In Run D, of 163 pairs situated near the 3:2 and 2:1 resonances with $-0.015 \leq \Delta \leq 0.03$ —these mostly include unmerged planets b:c, c:d, d:e, and f:g—there are 75 pairs with well-defined TTV phases and 88 pairs without well-defined phases. Those pairs without well-defined phases are frequently situated adjacent to another near-commensurate pair—the resonances interfere with one another to render their TTV time series non-sinusoidal, as is the case for resonant chains today like TOI-1136 (D23) and TRAPPIST-1 (Agol et al. 2021).

In the bottom row of Figure 13, we show the distribution of well-defined TTV phases from Run D. These are compared against phases calculated using observed TTVs from Rowe et al. (2015), as shown in the top row. The observed TTV phases are computed following the same procedure as described above, with $\max \Delta t_{\text{col}}$ set to the sum of the observed transit durations as given by the March 2024 NASA Exoplanet Archive. Of the 98 pairs of planets in the Archive with radii $< 4R_{\oplus}$ and $-0.015 \leq \Delta \leq 0.03$ near the 3:2 and 2:1 commensurabilities, there are 19 pairs with well-defined TTV phases, a percentage within a factor of 3 of that for Run D.

Figure 13 shows that our simulations can approximately reproduce the broad distribution of observed TTV phases. This is as expected, as the dynamical instabilities that lead to mergers and the breaking of resonant chains also perturb surviving resonant pairs. The resonant survivors are practically fated to have large TTV phases, as the chains start their lives with large libration amplitudes (Figure 5). Later major mergers, and minor mergers between resonant planets and debris particles, maintain free eccentricities and TTV phases. What is perhaps more noteworthy is that our model promises to generate large TTV phases while also producing the prominent 2:1 peak-trough

asymmetry in the period ratio histogram (Figure 3). In our scenario, there is not a single dissipative mechanism operating to create the peak-trough asymmetry, as such a mechanism acting alone would also damp TTV phases. Instead the peak and trough are built and maintained by multiple processes: first, disk-driven migration and eccentricity damping create only peaks at $\Delta > 0$; subsequent dynamical instabilities erode those peaks to form a continuum of period ratios, but one which does not extend to $\Delta < 0$ for the 2:1 resonance; and outside-grazing minor mergers (section 3.2) widen the trough and heighten the peak. All of this activity cannot help but knock resonant pairs off their fixed points, i.e. excite TTV phases.

5. SUMMARY AND DISCUSSION

We have tried to piece together the history of events leading to the unraveling of mean-motion resonant chains into which most if not all close-in sub-Neptunes are born. Major chapters remain missing, but our integrations have helped us identify themes if not also a few leads:

1. Resonant chains formed by convergent migration of planets in their parent disks cannot be too tightly bound, i.e. the resonant libration amplitudes (equivalently free eccentricities) of planet pairs cannot be too small. Otherwise the chains are too stable and do not break within system lifetimes, contrary to observation. This problem has been noted previously (Izidoro et al. 2017, 2021; for the giant planet case, see Nagpal et al. 2024). There does not seem to be a general understanding as to what is physically responsible for keeping libration amplitudes large—and not too large, lest the chains break too quickly compared to the observed destruction timescale of ~ 100 Myr. Possibilities include stochastic torques from turbulent disks (e.g. Rein & Liu 2012; Goldberg & Batygin 2023), mass loss from gas envelopes (e.g. Matsumoto & Ogihara 2020, Owen & Schlichting 2024), overstable librations from eccentricity damping (e.g. Goldreich & Schlichting 2014, Nesvorný et al. 2022), and scattering and collisions from planetesimals (e.g. Wu et al. 2024). Izidoro et al. (2021) found within their specific scenario of pebble accretion that their model parameters could be adjusted to produce more unstable chains having more planets crammed closer to disk inner edges and occupying higher-degree 1st-order resonances (e.g., 7:6, 6:5, 5:4; their section 5.3).

Our simulated chains either did not break (when initialized with the results of standard

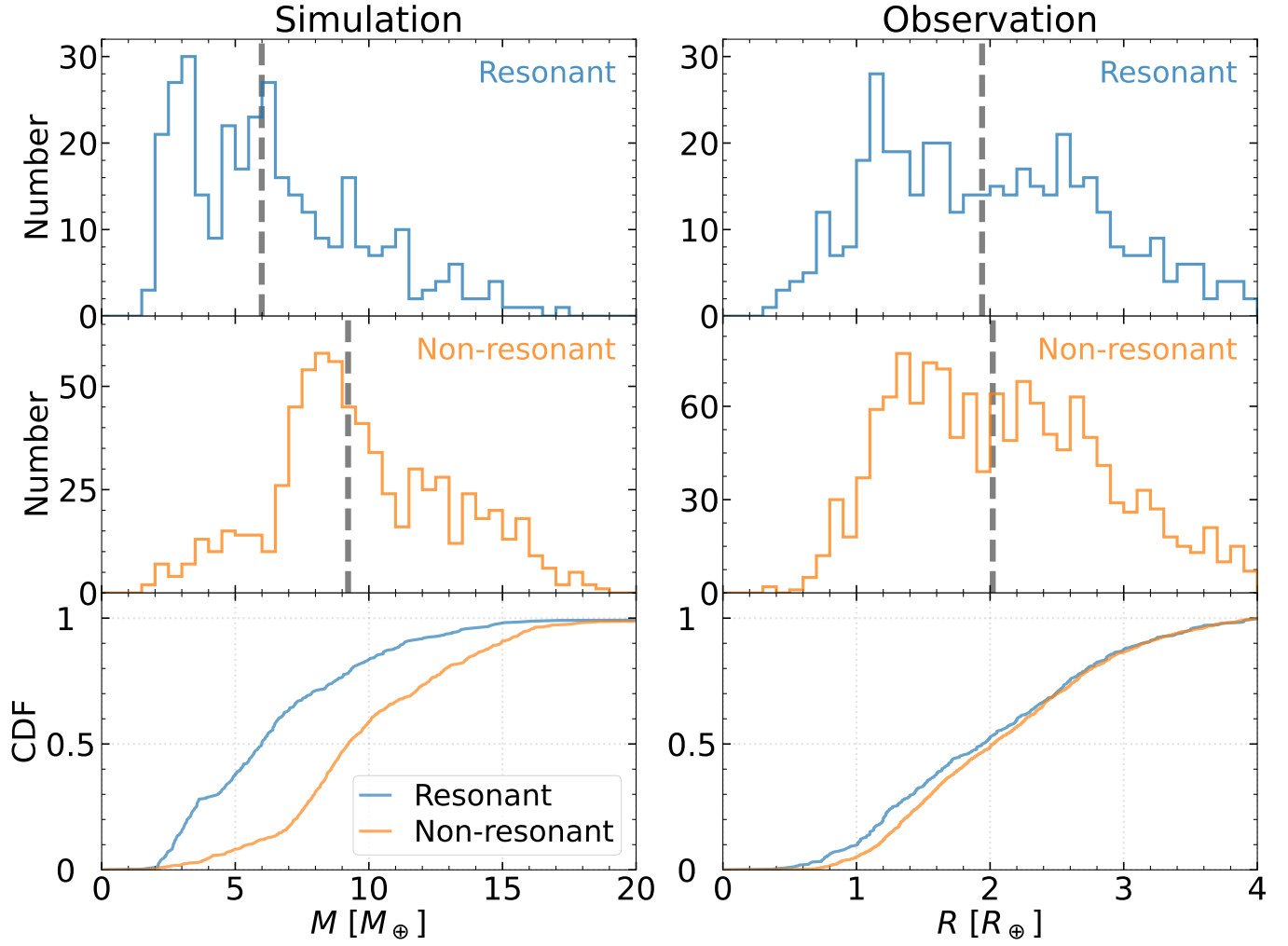


Figure 14. When resonant chains of close-in sub-Neptunes break, non-resonant planets are created from mergers and are more massive than resonant planets which survive mergers. This is borne out in our simulations (left column showing mass distributions from Run D; the bottom panel shows the cumulative distribution functions). It is not clear whether the *Kepler* observations, which measure radius instead of mass (right column, for planets with radii $R < 4R_{\oplus}$), support this prediction, as the radius distributions of resonant and non-resonant planets look largely similar (with a slight excess at $\sim 1R_{\oplus}$ for the resonant planets). Resonant planets are defined as those with $-0.015 < \Delta < 0.03$ for 1st order resonances and $-0.015 < \Delta < 0.015$ for 2nd order resonances. Median values are shown as dashed vertical lines.

disk-migration and eccentricity damping models) or broke too quickly (when initialized arbitrarily with parameters drawn from observations). Nonetheless our simulated outcomes for broken chains, evaluated at a time of 100 Myr, bore some resemblance to observations, as we detail below.

2. Second-order resonances such as the 7:5 may play a role in destabilizing resonant chains (see also Dai et al. 2023).
3. In the histogram of neighboring-planet period ratios P_2/P_1 (see Figure 3), the observed preference for 3:2 and 2:1 near-resonant *Kepler* planets to be situated just wide of resonance, and the observed deficit of systems just short of the 2:1 resonance

(and not the 3:2 resonance), may arise from the following sequence of events:

Stage (i): The resonant peaks in the P_2/P_1 histogram form when parent disks drive their planet progeny into chains comprising 3:2 and 2:1 resonances (in addition to an admixture of 2nd order resonances like the 7:5). Disk-driven migration and eccentricity damping forces these 1st order resonant pairs to librate about their fixed points which lie wide of perfect commensurability; the peaks are centered at $\Delta > 0$, where Δ is the fractional separation from an $(m+1):m$ period ratio (e.g. Goldreich 1965; Terquem & Papaloizou 2019; Choksi & Chiang 2020).

Stage (ii): Once the disk clears, dynamical instabilities over the next 100 Myr cause neighboring planets to merge, with merger products having orbital periods intermediate between those of their progenitors. Orbital spacings are thus widened. Merging members of a 3:2 resonant pair with planets outside the pair reduces the population in the 3:2 peak (without necessarily erasing the surviving 3:2 pairs’ preference for $\Delta > 0$), and forms a continuum of period ratios at $P_2/P_1 > 3/2$. An analogous continuum at $P_2/P_1 > 2$ forms from the erosion of the 2:1 peak. The continuum resulting from the erosion of a resonant peak has finite extent; its shape in period ratio space depends on the mass and orbital spacing distribution of the merger progenitors, and the chaotic history of their interactions prior to merging. If the continuum at $P_2/P_1 > 3/2$ drops off sufficiently at $P_2/P_1 = 2$ —and note that the distance between the 3:2 and 2:1 resonances is the largest among neighboring first-order resonances—then a “trough” (population deficit) appears at $\Delta < 0$ for the 2:1 resonance (Fig. 3). No trough appears for the 3:2 resonance, either because the distance between the 4:3 and 3:2 resonances is small enough to be bridged by the continuum formed by the erosion of the 4:3 peak, or because the original resonant chains formed in stage (i) do not feature large populations at $P_2/P_1 < 3/2$ (which seems likely insofar as planets capture into 3:2 before they capture into closer resonances like 4:3). The same reasoning avoids troughs for the 4:3, 5:4, and closer resonances.

Stage (iii): Planetesimal debris created from planetary mergers have their eccentricities increased by subsequent gravitational scatterings, to the point where the debris grazes the orbits of surviving resonant pairs from the outside. When such minor bodies collide with either member of a resonant pair, the pair’s orbital spacing is widened, further enhancing the population at $\Delta > 0$ at the expense of $\Delta < 0$ (fourth panel from the top in Figure 3).

Admittedly, this line of thinking is still schematic. The shapes of the period ratio continua produced by mergers need to be better understood. In particular the continua produced in our simulations by the erosion of the 3:2 and 2:1 peaks appear too bimodal (at least at 100 Myr) to match the smooth distribution observed for *Kepler* planets today. Our experiments are too

reliant on TOI-1136; mixing in other resonant chain architectures (different masses, different resonances, different eccentricities) will broaden the period ratio distributions. Encouragingly, in experiments with architectures other than TOI-1136 (e.g. TOI-178 and TRAPPIST-1), we repeatedly found 2:1 troughs (data not shown).

4. Free eccentricities in resonant pairs are excited at every stage of this history, both at the beginning, by whatever process kept resonant libration amplitudes large to cause the eventual breaking of resonant chains, and also during the ensuing protracted era of dynamical instabilities and giant impacts (major and minor mergers). Sub-Neptunes perturbed onto eccentric orbits may secularly force neighboring resonant pairs to be similarly eccentric, as shown by [Choksi & Chiang \(2023\)](#) (in their mechanism, the secularly forced eccentricity from the third-body perturber becomes the resonant pair’s free eccentricity). All of this activity and violence is recorded (and likely overwritten) in the transit timing variations (TTVs) of surviving resonant pairs. If those resonant pairs are sufficiently isolated from other mean-motion resonances with other surviving planets, their TTVs will be simple sinusoids with large phases—as observed.
5. A simple prediction of mergers destroying resonant chains is that non-resonant planets, being merger products, should be more massive than resonant planets, which are unmerged survivors of dynamical instability. Figure 14 verifies that this is the case for our simulations (left column); for the simulations we plot mass instead of radius, because radius depends sensitively on gas content, which can change with giant impacts (e.g. [Yalinewich & Schlichting 2019](#)), and which our simulations do not track. Conversely, for the observations, Figure 14 plots the observable radius instead of the model-dependent mass (right column). At the moment the observational evidence that mature resonant planets are larger than non-resonant planets does not seem statistically significant, though at least it appears to have the right sign.

ACKNOWLEDGEMENTS

R.L. thanks Dong Lai, Chris Ormel, Sharon Xuesong Wang, and Wei Zhu for useful exchanges, and

acknowledges support from the Heising-Simons Foundation 51 Pegasi b Fellowship. E.C. was supported by NSF grant 2205500 and the Simons Foundation Investigator program.

Software: Rebound (Rein & Liu 2012; Rein et al. 2019; Rein & Tamayo 2017; Lu et al. 2024), Matplotlib (Hunter 2007), Numpy & Scipy (Jones et al. 2001).

REFERENCES

- Aarseth, S. J., Lin, D. N. C., & Palmer, P. L. 1993, ApJ, 403, 351, doi: [10.1086/172208](https://doi.org/10.1086/172208)
- Agol, E., Dorn, C., Grimm, S. L., et al. 2021, PSJ, 2, 1, doi: [10.3847/PSJ/abd022](https://doi.org/10.3847/PSJ/abd022)
- Batygin, K., & Morbidelli, A. 2013, AJ, 145, 1, doi: [10.1088/0004-6256/145/1/1](https://doi.org/10.1088/0004-6256/145/1/1)
- Cambioni, S., Asphaug, E., Emsenhuber, A., et al. 2019, ApJ, 875, 40, doi: [10.3847/1538-4357/ab0e8a](https://doi.org/10.3847/1538-4357/ab0e8a)
- Choksi, N., & Chiang, E. 2020, MNRAS, 495, 4192, doi: [10.1093/mnras/staa1421](https://doi.org/10.1093/mnras/staa1421)
- . 2023, MNRAS, 522, 1914, doi: [10.1093/mnras/stad835](https://doi.org/10.1093/mnras/stad835)
- Dai, F., Masuda, K., Beard, C., et al. 2023, AJ, 165, 33, doi: [10.3847/1538-3881/aca327](https://doi.org/10.3847/1538-3881/aca327)
- Dai, F., Goldberg, M., Batygin, K., et al. 2024, arXiv e-prints, arXiv:2406.06885, doi: [10.48550/arXiv.2406.06885](https://doi.org/10.48550/arXiv.2406.06885)
- Emsenhuber, A., & Asphaug, E. 2019, ApJ, 875, 95, doi: [10.3847/1538-4357/ab0c1d](https://doi.org/10.3847/1538-4357/ab0c1d)
- Emsenhuber, A., Cambioni, S., Asphaug, E., et al. 2020, ApJ, 891, 6, doi: [10.3847/1538-4357/ab6de5](https://doi.org/10.3847/1538-4357/ab6de5)
- Esteves, L., Izidoro, A., Bitsch, B., et al. 2022, MNRAS, 509, 2856, doi: [10.1093/mnras/stab3203](https://doi.org/10.1093/mnras/stab3203)
- Fabrycky, D. C., Lissauer, J. J., Ragozzine, D., et al. 2014, ApJ, 790, 146, doi: [10.1088/0004-637X/790/2/146](https://doi.org/10.1088/0004-637X/790/2/146)
- Gabriel, T. S. J., & Cambioni, S. 2023, Annual Review of Earth and Planetary Sciences, 51, 671, doi: [10.1146/annurev-earth-031621-055545](https://doi.org/10.1146/annurev-earth-031621-055545)
- Goldberg, M., & Batygin, K. 2022, AJ, 163, 201, doi: [10.3847/1538-3881/ac5961](https://doi.org/10.3847/1538-3881/ac5961)
- . 2023, ApJ, 948, 12, doi: [10.3847/1538-4357/acc9ae](https://doi.org/10.3847/1538-4357/acc9ae)
- Goldberg, M., Batygin, K., & Morbidelli, A. 2022, Icarus, 388, 115206, doi: [10.1016/j.icarus.2022.115206](https://doi.org/10.1016/j.icarus.2022.115206)
- Goldreich, P. 1965, MNRAS, 130, 159, doi: [10.1093/mnras/130.3.159](https://doi.org/10.1093/mnras/130.3.159)
- Goldreich, P., & Sari, R. 2003, ApJ, 585, 1024, doi: [10.1086/346202](https://doi.org/10.1086/346202)
- Goldreich, P., & Schlichting, H. E. 2014, AJ, 147, 32, doi: [10.1088/0004-6256/147/2/32](https://doi.org/10.1088/0004-6256/147/2/32)
- Hadden, S., & Lithwick, Y. 2014, ApJ, 787, 80, doi: [10.1088/0004-637X/787/1/80](https://doi.org/10.1088/0004-637X/787/1/80)
- Hunter, J. D. 2007, Computing in Science Engineering, 9, 90, doi: [10.1109/MCSE.2007.55](https://doi.org/10.1109/MCSE.2007.55)
- Izidoro, A., Bitsch, B., Raymond, S. N., et al. 2021, A&A, 650, A152, doi: [10.1051/0004-6361/201935336](https://doi.org/10.1051/0004-6361/201935336)
- Izidoro, A., Ogihara, M., Raymond, S. N., et al. 2017, MNRAS, 470, 1750, doi: [10.1093/mnras/stx1232](https://doi.org/10.1093/mnras/stx1232)
- Jensen, D., & Millholland, S. C. 2022, AJ, 164, 144, doi: [10.3847/1538-3881/ac86c5](https://doi.org/10.3847/1538-3881/ac86c5)
- Jones, E., Oliphant, T., Peterson, P., et al. 2001, SciPy: Open source scientific tools for Python. <http://www.scipy.org/>
- Jontof-Hutter, D., Ford, E. B., Rowe, J. F., et al. 2016, ApJ, 820, 39, doi: [10.3847/0004-637X/820/1/39](https://doi.org/10.3847/0004-637X/820/1/39)
- Leinhardt, Z. M., & Stewart, S. T. 2012, ApJ, 745, 79, doi: [10.1088/0004-637X/745/1/79](https://doi.org/10.1088/0004-637X/745/1/79)
- Leleu, A., Alibert, Y., Hara, N. C., et al. 2021, A&A, 649, A26, doi: [10.1051/0004-6361/202039767](https://doi.org/10.1051/0004-6361/202039767)
- Lissauer, J. J., Ragozzine, D., Fabrycky, D. C., et al. 2011, ApJS, 197, 8, doi: [10.1088/0067-0049/197/1/8](https://doi.org/10.1088/0067-0049/197/1/8)
- Lithwick, Y., & Wu, Y. 2012, ApJL, 756, L11, doi: [10.1088/2041-8205/756/1/L11](https://doi.org/10.1088/2041-8205/756/1/L11)
- Lithwick, Y., Xie, J., & Wu, Y. 2012, ApJ, 761, 122, doi: [10.1088/0004-637X/761/2/122](https://doi.org/10.1088/0004-637X/761/2/122)
- Lu, T., Hernandez, D. M., & Rein, H. 2024, arXiv e-prints, arXiv:2405.03800, doi: [10.48550/arXiv.2405.03800](https://doi.org/10.48550/arXiv.2405.03800)
- MacDonald, M. G., Ragozzine, D., Fabrycky, D. C., et al. 2016, AJ, 152, 105, doi: [10.3847/0004-6256/152/4/105](https://doi.org/10.3847/0004-6256/152/4/105)
- Matsumoto, Y., & Ogihara, M. 2020, ApJ, 893, 43, doi: [10.3847/1538-4357/ab7cd7](https://doi.org/10.3847/1538-4357/ab7cd7)
- Mills, S. M., Fabrycky, D. C., Migaszewski, C., et al. 2016, Nature, 533, 509, doi: [10.1038/nature17445](https://doi.org/10.1038/nature17445)
- Nagpal, V., Goldberg, M., & Batygin, K. 2024, ApJ, 969, 133, doi: [10.3847/1538-4357/ad3046](https://doi.org/10.3847/1538-4357/ad3046)
- Nesvorný, D., Chrenko, O., & Flock, M. 2022, ApJ, 925, 38, doi: [10.3847/1538-4357/ac36cd](https://doi.org/10.3847/1538-4357/ac36cd)
- Owen, J. E., & Schlichting, H. E. 2024, MNRAS, 528, 1615, doi: [10.1093/mnras/stad3972](https://doi.org/10.1093/mnras/stad3972)
- Rein, H., & Liu, S. F. 2012, A&A, 537, A128, doi: [10.1051/0004-6361/201118085](https://doi.org/10.1051/0004-6361/201118085)
- Rein, H., & Liu, S.-F. 2012, A&A, 537, A128, doi: [10.1051/0004-6361/201118085](https://doi.org/10.1051/0004-6361/201118085)
- Rein, H., & Tamayo, D. 2017, MNRAS, 467, 2377, doi: [10.1093/mnras/stx232](https://doi.org/10.1093/mnras/stx232)
- Rein, H., Hernandez, D. M., Tamayo, D., et al. 2019, MNRAS, 485, 5490, doi: [10.1093/mnras/stz769](https://doi.org/10.1093/mnras/stz769)

- Ricker, G. R., Winn, J. N., Vanderspek, R., et al. 2014, in Society of Photo-Optical Instrumentation Engineers (SPIE) Conference Series, Vol. 9143, Space Telescopes and Instrumentation 2014: Optical, Infrared, and Millimeter Wave, ed. J. Oschmann, Jacobus M., M. Clampin, G. G. Fazio, & H. A. MacEwen, 914320, doi: [10.1117/12.2063489](https://doi.org/10.1117/12.2063489)
- Rowe, J. F., Coughlin, J. L., Antoci, V., et al. 2015, ApJS, 217, 16, doi: [10.1088/0067-0049/217/1/16](https://doi.org/10.1088/0067-0049/217/1/16)
- Tamayo, D., Rein, H., Shi, P., & Hernandez, D. M. 2020, MNRAS, 491, 2885, doi: [10.1093/mnras/stz2870](https://doi.org/10.1093/mnras/stz2870)
- Terquem, C., & Papaloizou, J. C. B. 2019, MNRAS, 482, 530, doi: [10.1093/mnras/sty2693](https://doi.org/10.1093/mnras/sty2693)
- Teyssandier, J., Libert, A. S., & Agol, E. 2022, A&A, 658, A170, doi: [10.1051/0004-6361/202142377](https://doi.org/10.1051/0004-6361/202142377)
- Weisserman, D., Becker, J. C., & Vanderburg, A. 2023, AJ, 165, 89, doi: [10.3847/1538-3881/acac80](https://doi.org/10.3847/1538-3881/acac80)
- Wu, Y., & Lithwick, Y. 2013, ApJ, 772, 74, doi: [10.1088/0004-637X/772/1/74](https://doi.org/10.1088/0004-637X/772/1/74)
- Wu, Y., Malhotra, R., & Lithwick, Y. 2024, arXiv e-prints, arXiv:2405.08893, doi: [10.48550/arXiv.2405.08893](https://doi.org/10.48550/arXiv.2405.08893)
- Yalinewich, A., & Schlichting, H. 2019, MNRAS, 486, 2780, doi: [10.1093/mnras/stz1049](https://doi.org/10.1093/mnras/stz1049)